Appl. Phys. B 87, 431–436 (2007)
DOI: 10.1007/s00340-007-2608-8

Applied Physics B
Lasers and Optics

A. SAHA[2]
A. RAY[1]
S. MUKHOPADHYAY[1,*]
P.K. DATTA[1,✉]
P.K. DUTTA[2]
S.M. SALTIEL[3]

Littrow-type discretely tunable, *Q*-switched Nd:YAG laser around 1.3 μm

[1] Department of Physics and Meteorology, Indian Institute of Technology, Kharagpur 721302, India
[2] Department of Electrical Engineering, Indian Institute of Technology, Kharagpur 721302, India
[3] Faculty of Physics, University of Sofia, 5 J. Bourchier Boulevard, 1164 Sofia, Bulgaria

Received: 5 July 2006/Revised version: 22 January 2007
Published online: 31 March 2007 • © Springer-Verlag 2007

ABSTRACT An all-solid-state, side diode array pulse pumped Nd:YAG laser tunable for six wavelengths ranging from 1318.8 nm to 1356.0 nm is developed. The tunability is obtained by using a grating in Littrow mode that also serves as an output coupler. The configuration ensures a line width as low as 0.04 nm. Thermal effects limit the maximum average power to 250 mW for an average absorbed pump power of 8.0 W in the free-running condition. An acousto-optic *Q*-switching of the laser provides pulses of width 251 ns with peak power of 733 W for an average pump power of 11.5 W. The laser may find application in microsurgery and dermatology.

PACS 42.55.Xi; 42.60.-v; 42.60.Fc; 42.60.Gd; 42.62.Be

1 Introduction

The laser radiation with wavelengths around 1.3 μm is recently being employed in surgical processes. The Nd:YAG lasers at 1.3 μm are being preferred to that of 1.064 μm owing to a 10-fold higher absorption in water and one-third extinction in blood, so the desired effects of cutting capability, coagulation and fistula sealing can be achieved only with this laser. Recently, lung parenchyma resections were reported using a Nd:YAG laser operating around 1.3 μm [1–3]. The Nd:YAG laser around 1.3 μm is also a potential source for neurosurgery [4, 5] and also for treatment of acne scars as it minimizes epidermal damage by cooling the epidermis while targeting within the dermis at its active chromophore [6, 7]. Although most of the recent works involve lasers at 1318 nm, other wavelengths such as 1338 nm and 1356 nm can be more useful as they have higher absorption in water. The alternative approach for sources of tunable coherent radiation, such as optical parametric oscillators, suffer from wide line width, low output power and require very high power pump sources for continuous-wave (cw) operation.

✉ Fax: +91-3222-255303, E-mail: pkdatta@phy.iitkgp.ernet.in
*Present address: Hooghly Mohsin College, West Bengal, India

Nd:YAG crystal has several dozen transition lines and laser emissions are feasible in most of these transition lines [8]. The energy levels of the rare-earth elements (Nd^{3+}) split into a number of Stark levels due to the action of the crystal field. The electron transition corresponding to each Stark level emits a different wavelength. The Nd^{3+} ion in YAG host exhibits transitions in the vicinity of 1.3 μm corresponding to ${}^4F_{3/2} \rightarrow {}^4I_{13/2}$ that are $R_2 \rightarrow X_1$, $R_2 \rightarrow X_3$, $R_2 \rightarrow X_2$, $R_1 \rightarrow X_1$, $R_1 \rightarrow X_2$, $R_2 \rightarrow X_4$ and $R_1 \rightarrow X_4$ leading to laser radiation around 1318.8 nm, 1338.2 nm, 1320.0 nm, 1333.8 nm, 1335.0 nm, 1341.0 nm and 1356.4 nm, respectively. These energy levels are shown in Fig. 1.

The rare earth element doped solid state lasers generally oscillate at one wavelength due to the difference of their stimulated emission cross section, fluorescence lifetime and fluorescence quantum efficiency. Generally, the strongest laser transition suppresses the other transitions. However, the desired wavelength can be made to oscillate by using dispersive cavity elements, such as prisms, etalons, birefringent tuners or gratings.

An acousto-optically *Q*-switched Nd:$YAlO_3$ laser discretely tunable in the range from 1064 nm to 1099 nm was reported using birefringent tuners [9]. Stoneman and Esterowitz increased the range of tunability in Ti:sapphire laser pumped Tm:YAG and Tm:YSGG lasers continuously tunable over the ranges 1870–2160 nm and 1850–2140 nm respectively for cw mode of operation using birefringent tuners [10]. Ter-Mikirtychnevan and Fromzel demonstrated tunability in a wavelength range of 1047–1051 nm for a cw single-diode-pumped Yb:YAG laser with a line width of 1.5–2.1 GHz using an etalon as a tuner [11]. The line width was reduced in a single-frequency Yb:YAG laser tunable from 1028 nm to 1031 nm with a line width less than 1.5 GHz using a 116-μm-thick etalon as a tuner [12]. Marling tuned 19 different transitions from 1052 nm to 1444 nm in a arc lamp pumped Nd:YAG laser in cw mode with two solid etalons having thicknesses of 0.1 mm and 0.5 mm [13]. The line width was drastically reduced in a grating tuned single longitudinal mode diode pumped Nd:YVO_4 laser operating around 1064 nm [14]. Recently, electro-optic wavelength tuning of the order of 94 pm of a Ti:sapphire laser was reported using a $LiNbO_3$ prism with an electric field of 10 kV/cm

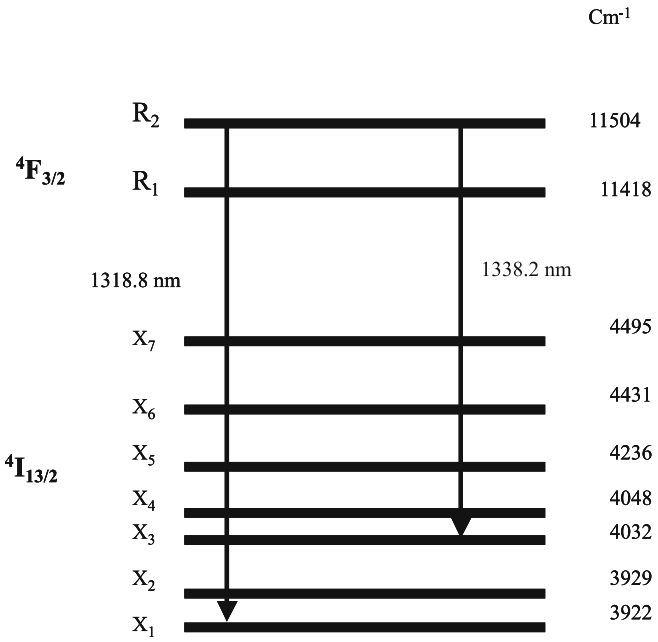

FIGURE 1 Stark splitting of $^4F_{3/2}$ and $^4I_{13/2}$ of Nd^{3+} ion in YAG host

and a separate grating [15]. Tunable simultaneous multi-wavelength operation of a Nd:YAG laser around 1.06 μm was achieved using four prisms [16]. Recently, we reported simultaneous multi-wavelength oscillation of a Nd:YAG laser around 1.32 μm [17]. There are also some reports of the cw and Q-switched operation of Nd:YAG lasers around 1.3 μm [18–20]. The use of prisms leads to thermally induced birefringence that induces losses in the laser cavities with polarizing elements. The stress-induced birefringence is also very common in prisms because of the inhomogeneous density occurring during the growth of the glass. When high-power radiation is incident on it, birefringence may be enhanced due to the inhomogeneous thermo-optic coefficient. Because of the low thermal conductivity the temperatures within the volume of a glass piece cannot follow the changing environmental temperatures quickly and therefore significant temperature differences arise between different volume regions. The high values of Young's modulus and the coefficients of thermal expansion for the optical glasses consequently lead to thermally induced stresses in the glass volume. Such losses can be avoided by using etalons or gratings for tuning. In this article we report the first, to the best of our knowledge, all-solid-state, side diode array pulse pumped Nd:YAG laser tunable for six wavelengths ranging from 1318.8 nm to 1356.0 nm. Here we use an intracavity telescope and a grating in Littrow configuration to oscillate a Nd:YAG laser around 1.3 μm with reduced line width, both in quasi-cw and Q-switched modes. We also study the thermal effects on the Nd:YAG rod and its implication on the laser oscillations. Compared to the Littrow cavity, the Littman–Metcalf design, which uses a grating at near-grazing incidence and where the first-order diffracted beam is reflected back to the cavity by an additional mirror, has a more complex design, lower output efficiency and requires extra cavity components [21]. The significance of this oscillator lies in its compact geometry, tunability and simplicity.

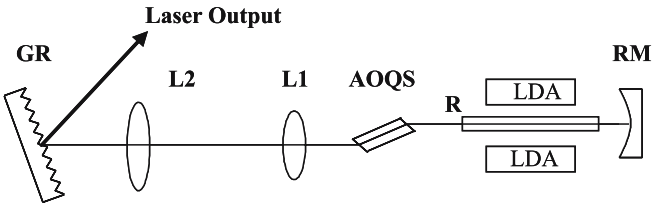

FIGURE 2 Laser layout: LDA – laser diode array; RM – rear mirror; AOQS – acousto-optic Q-switch; GR – grating; R – Nd:YAG rod; L1, L2 – lenses

2 Experiment

The schematic diagram of the laser is shown in Fig. 2. A Nd:YAG rod of length 63 mm and diameter 2 mm with Nd^{3+} doping concentration of 0.6% is used as the gain medium. The central 32 mm of the rod is effectively pumped radially by 18 temperature-tuned pulsed laser diode bars emitting at the wavelength of 808 nm. There are three arrays of laser diode bars placed radially 120° apart. Each array consists of six diode bars in a 3×2 matrix. The laser diode bars are designed for quasi-cw operation. The pump pulse duration and the repetition rate can be varied over the ranges of 50–550 μs and 50 Hz–1 kHz, respectively. For our experiment, the pump pulse width and the pulse-repetition rate were kept fixed at 200 μs and 200 Hz, respectively. The rear mirror (RM) is concave, with radius of curvature of 500 mm and reflectivity of 99.5% in the wavelength range 1300 nm to 1400 nm and has a high transmittance ($T = 93\%$) at 1064 nm that prevented the generation at this wavelength. A diffraction grating (GR) with 600 rulings per mm and blazed at 1064 nm is used as an output coupler. The first order diffraction maximum of the grating is used as the positive feedback in the cavity while the central maximum is used as an output of the laser. Two lenses L1 and L2 are used in telescopic configuration to produce a laser mode diameter of 5 mm and 1 mm at the grating and at the center of the gain medium, respectively. The configuration enables us to achieve good spectral resolution at the laser output as well as helps running the laser in single transverse mode. The lenses L1 and L2 with focal lengths of 50 mm and 300 mm are placed with a separation of 345 mm. The cavity length is optimized at 675 mm for lowest order single transverse mode operation as well as for low-bandwidth operation of the laser. To measure the output wavelength, a 0.67-m-long (focal length) monochromator (Macpherson Inc., USA) with a resolution of 0.2 nm (FWHM) is used.

The power absorbed by the Nd:YAG rod is given by $P_{ab} = \eta_T \eta_A \eta_S \eta_Q \eta_B P_{op}$. The available optical power from the diode array (P_{op}) $= \eta_P \times P_{el}$ and the average input electrical power (P_{el}) = diode bias voltage × drive peak current × duty cycle (pulse width × repetition rate), where the coefficients have their usual meaning [8]. For our operating condition the peak power from the diode array at a current of 45 A is about 594 W for a duration of 200 μs, corresponding to an average power of 23.8 W. The peak power from each diode bar is 33 W.

Q-switching of the laser is realized by using a fused-silica acousto-optic Q-switch (AOQS) (Neos Technologies Inc., USA). The AOQS is Brewster cut for 1064 nm and is driven by a radio-frequency signal of 27.2 MHz with a modulation in the frequency range 1–50 kHz. A 500-MHz digital storage oscilloscope (Tektronix 3054A) is used to measure the

Q-switch pulse width after detection with an InGaAs photodiode (FCI-100L, OSI Fibercomm Inc.).

3 Thermal effects

Thermal effects are very important in scaling the diode-pumped solid-state lasers as they limit the maximum pump power. Heat is dissipated in the gain medium primarily due to the quantum defect, which is the difference between the pump photon energy and the laser photon energy divided by the pump photon energy. Apart from the quantum defect, the non-radiative transitions associated with the cross-relaxation and re-absorption processes lead to heat dissipation inside the gain medium. But, their contribution to the heat generation in the gain medium is small compared to the quantum defect. The fraction of heat dissipated in the gain medium due to the quantum defect is given as

$$\eta_{\mathrm{h}} = \left(1 - \frac{\nu_{\mathrm{L}}}{\nu_{\mathrm{P}}}\right), \tag{1}$$

where ν_{L} and ν_{P} are the laser photon frequencies and the pump photon frequencies, respectively. For the side-pumped cylindrical Nd:YAG rod the radial temperature distribution is given by [8]

$$\frac{1}{r}\left(\frac{\partial T}{\partial r}\right) + \frac{\partial^2 T}{\partial r^2} = -\frac{Q}{K}. \tag{2}$$

Here K is the thermal conductivity and Q is the rate of heat generation per unit volume:

$$Q = \left(\frac{\eta_{\mathrm{h}} P_{\mathrm{abs}}}{\pi r_0^2 l}\right). \tag{3}$$

If $T(r_0)$ is the temperature at the boundary of the Nd:YAG rod, the steady-state radial temperature distribution as obtained from (2) is

$$T(r) = T(r_0) + \left(\frac{Q}{4K}\right)\left(r_0^2 - r^2\right). \tag{4}$$

The radial change in the refractive index due to the temperature difference is given as

$$n(r) = n_0 + \Delta n(r)_T + \Delta n(r)_\varepsilon, \tag{5}$$

where n_0 is the refractive index at room temperature and $\Delta n(r)_T$ and $\Delta n(r)_\varepsilon$ are the temperature-dependent and stress-dependent changes in the refractive index of the rod. The temperature gradient generates mechanical stresses in the laser rod since the hotter inside area is constrained from expansion by the relatively cooler outer area. This stress in turn generates thermal strains in the rod, which in turn produce a refractive-index variation via the photoelastic effect. This leads to the extra term $\Delta n(r)_\varepsilon$. We have

$$\Delta n(r)_T = [T(r) - T(0)]\left(\frac{\mathrm{d}n}{\mathrm{d}T}\right) = -\frac{Q}{4K}\frac{\mathrm{d}n}{\mathrm{d}T}r^2, \tag{6}$$

$$\Delta n(r)_\varepsilon = -\frac{1}{2}n_0^3\frac{\alpha_T Q}{K}C_r r^2. \tag{7}$$

Here α_T is the thermal expansion coefficient and C_r the photoelastic coefficient. The net refractive index as obtained from (5) now becomes

$$n(r) = n_0\left[1 - \frac{Q}{2K}\left(\frac{1}{2n_0}\frac{\mathrm{d}n}{\mathrm{d}T} + n_0^2\alpha_T C_r\right)r^2\right] = n_0 - \frac{1}{2}n_r r^2. \tag{8}$$

In the above equation, we do not take into account the distortion of the end-face curvature of the rod. The change in the phase distortion due to this end-face curvature correction is negligible. The resulting thermal lens is similar to the GRIN lens and has a parabolic refractive-index profile as a radial function. The focal length of this type of lens is given as

$$f_T = \frac{KA}{\eta_{\mathrm{h}} P_{\mathrm{abs}}}\left(\frac{1}{2}\frac{\mathrm{d}n}{\mathrm{d}T} + \alpha_T C_r n_0^3\right)^{-1}. \tag{9}$$

The focal length of the thermal lens is calculated from (9) with the values [8]: $\mathrm{d}n/\mathrm{d}T = 7.3 \times 10^{-6}\,\mathrm{K}^{-1}$, $\alpha_T = 7.5 \times 10^{-6}\,\mathrm{K}^{-1}$, $n_0 = 1.8$, $K = 14\,\mathrm{W\,m^{-1}\,{}^{\circ}C^{-1}}$ and $C_r = 0.0172$ and is shown in Fig. 3.

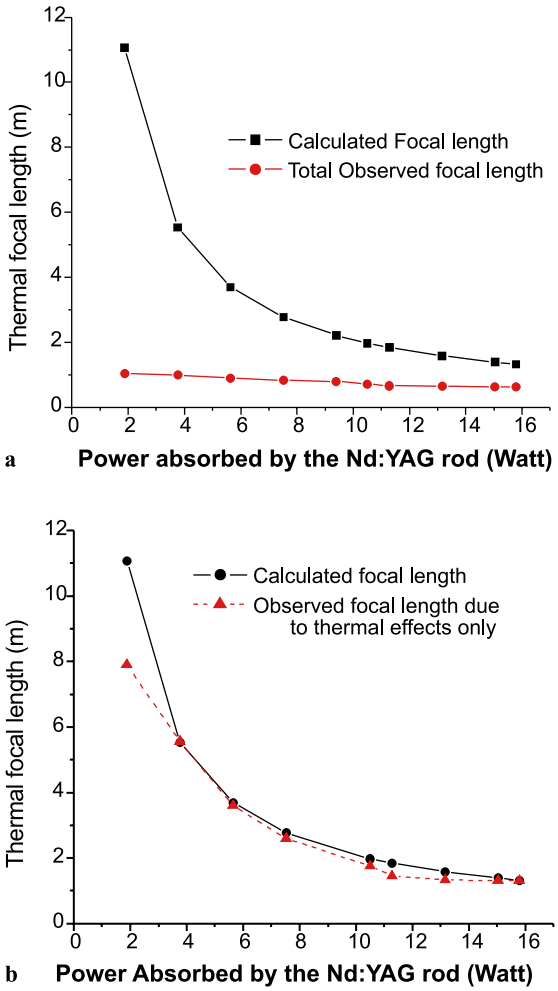

FIGURE 3 (**a**) The observed and calculated focal lengths of the thermal lens due to the heating of the Nd:YAG rod. (**b**) The measured focal length of the thermal lens after subtracting the contribution due to the mechanical effects

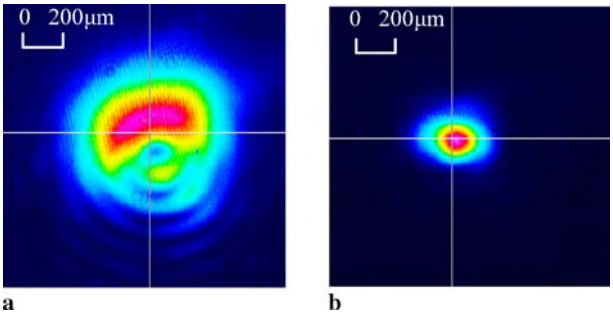

FIGURE 4 (**a**) The image of the He-Ne beam after passing through the Nd:YAG rod for a pump power of 4 W. (**b**) The image of the He-Ne beam after passing through the Nd:YAG rod for a pump power of 11 W

The thermal lensing effect in the Nd:YAG rod was monitored by passing a He-Ne laser beam through it. The observed change in the focal length is drawn in Fig. 3a. We find a clear discrepancy between the observed and calculated values. This is due to the fact that apart from the thermal effects, the mechanical stresses due to other factors like mounting of the crystal give rise to a change in the refractive-index profile across the medium [22, 23]. Mechanical stresses due to absorbed pump power are taken care of by the thermal lens itself.

Assuming that the separation between the lenses formed due to the two effects is very small, the net focal length of the gain medium can be computed from the equation

$$\frac{1}{f_e} = \frac{1}{f_T} + \frac{1}{f_{\text{mechanical}}} = \alpha P_{\text{abs}} + \beta\,, \tag{10}$$

where $\beta = 1/f_{\text{mechanical}}$ and α is a constant that can be obtained from (9).

In order to obtain only the thermal contribution, we plot the measured values of $1/f_e$ vs the absorbed pump power. The intercept of the curve on the Y axis gives us the value of β, which is the inverse of the mechanical focal length. Using (10), we obtain the thermal contribution (f_T) of the observed focal length by subtracting β from the value of $1/f_e$. The observed and calculated values of the thermal focal length (f_T) of the Nd:YAG rod as a function of the absorbed pump power are shown in Fig. 3b. In order to minimize thermal lensing effects, the cavity was optimized with suitable cavity components for maximizing the beam cross section on the Nd:YAG rod and the grating. The sharp variation of the diameter of the He-Ne beam at the end face of the Nd:YAG rod with the increase of the input pump power is shown in Fig. 4a and b.

4 Result and discussion

The laser is tuned by rotating the grating to produce six different wavelengths at 1318.8 nm, 1333.8 nm, 1335.0 nm, 1338.2 nm, 1341.0 nm and 1356.4 nm in both Q-switched and free-running operation. The laser radiation corresponding to the wavelength of 1320 nm is not detected. This is due to the fact that the gain cross section and branching ratio (defined as the number of photons emitted in a particular line divided by the total number of photons emitted) are very small for the line at 1320 nm. The power

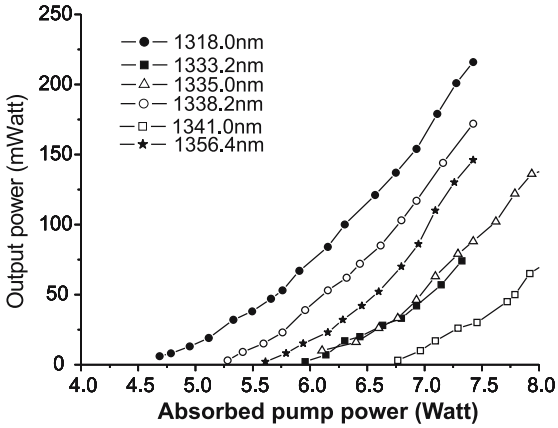

FIGURE 5 Average output power for the different lasing lines with absorbed pump power (by varying diode current) corresponding to the pump pulse repetition rate of 200 Hz

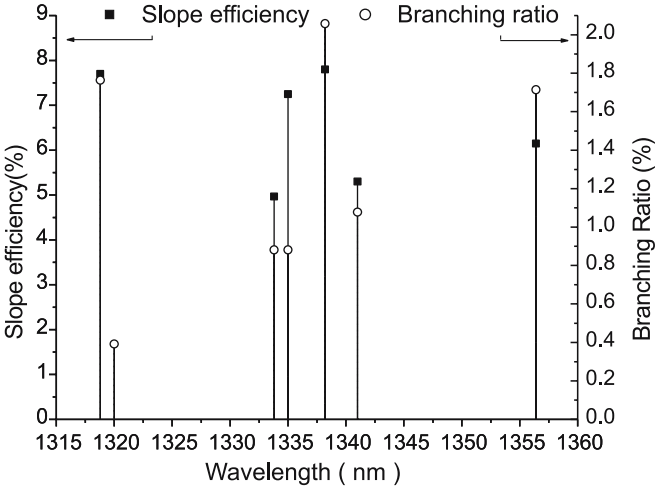

FIGURE 6 The slope efficiency and the branching ratio for each oscillating wavelength

scaling of the output of the laser with the absorbed pump power by varying the diode current in the free-running condition is shown in Fig. 5. During the entire experiment the pump pulse width and the pulse-repetition rate are kept fixed at 200 μs and 200 Hz, respectively. In the lasing regime, $P_{\text{out}} = \eta_{\text{diff}}(P_{\text{abs}} - P_{\text{threshold}})$ where, η_{diff} is the slope efficiency and is proportional to the branching ratio. The slope efficiencies and the branching ratios corresponding to the oscillating wavelengths are shown in Fig. 6. The very small branching ratio [24] for 1320 nm explains the absence of this weak line. Further, power could not be increased due to the thermal lensing effects in the Nd:YAG rod. As compared to the work in [17], we obtain a much lower efficiency due to the following reasons. The two lenses used as a beam expander for better resolution in the grating are uncoated, resulting in a single-pass loss of at least 4% from each surface. Moreover, the grating used in the experiment is blazed for 1064 nm, resulting in reduced coupling for the wavelength around 1.3 μm.

The line width is measured by setting up a Michelson interferometer. For this purpose two metal-coated mirrors and a cubic beam splitter are used. The circular interference fringes are observed using a highly sensitive infrared card.

The line width at 1318 nm is measured to be 0.04 nm, corresponding to the coherence length of about 2.0 cm.

This measured value can be compared with the theoretical estimation. Indeed, for a Gaussian beam, the angular divergence of the collimated beam that diffracts from the grating can be described by the far-field angle

$$\Delta\theta_1 = \frac{\lambda}{\pi\omega_1}, \tag{11}$$

where ω_1 is the beam waist after optimum collimation. The angular dispersion of a diffraction grating in Littrow mount is given by

$$\frac{\mathrm{d}\theta}{\mathrm{d}\lambda} = \frac{2\tan\theta}{\lambda}, \tag{12}$$

where θ is the angle of incidence. In order to displace the back-reflected beam passing through the telescope in a reverse direction by the same waist size on the gain medium, the deflection angle at the grating must be at least equal to the beam divergence. The wavelength spread within the allowed beam divergence is given by [25]

$$\Delta\lambda = \frac{\lambda^2}{2\pi\omega_1\tan\theta}. \tag{13}$$

The calculated value of the passive line width is about 0.24 nm, which is large compared to the measured value of 0.04 nm by the Micheleson interferometer. Such a one order of magnitude discrepancy may be attributed to the fact that the calculated value is for a single pass through the grating, whereas the measured value is additionally narrowed due to the generation process. Inserting another dispersive element like a Fabry–Perot etalon or a Lyot filter inside the cavity can narrow the line width further. These methods are used to isolate only a single axial cavity mode. But, the use of these dispersive elements causes huge losses in the cavity, resulting in a sharp drop in the output power.

Q-switched operation of the laser is realized by using a fused-silica acousto-optic modulator. The Brewster-cut AOQS is driven by a radio-frequency signal of 27.2 MHz with a modulation in the frequency range of 1–50 kHz. To realize maximum diffraction efficiency from the cavity grating with vertical ruling, the Q-switch is placed to select the horizontal polarization, which is then orthogonal with the grooves of the cavity grating. The Q-switch threshold is found to increase because of the additional loss from the fused-silica modulator. For a given pump power, the average output power for each wavelength in Q-switched operation is about 80% of the power corresponding to the free-running condition. The thermal lensing effect decreases due to the increase in the beam size, allowing us to work with the absorbed pump power up to 12 W without saturating the laser output. The Q-switch pulses of width of 251 ns are obtained for a modulation frequency of 37 kHz. The oscilloscope traces of the pulses in different time scales are shown in Fig. 7a and b. There are about eight Q-switched pulses within one pump pulse. For stable operation, the limiting Q-switch modulation frequency for the acousto-optic modulator is 25 kHz. As

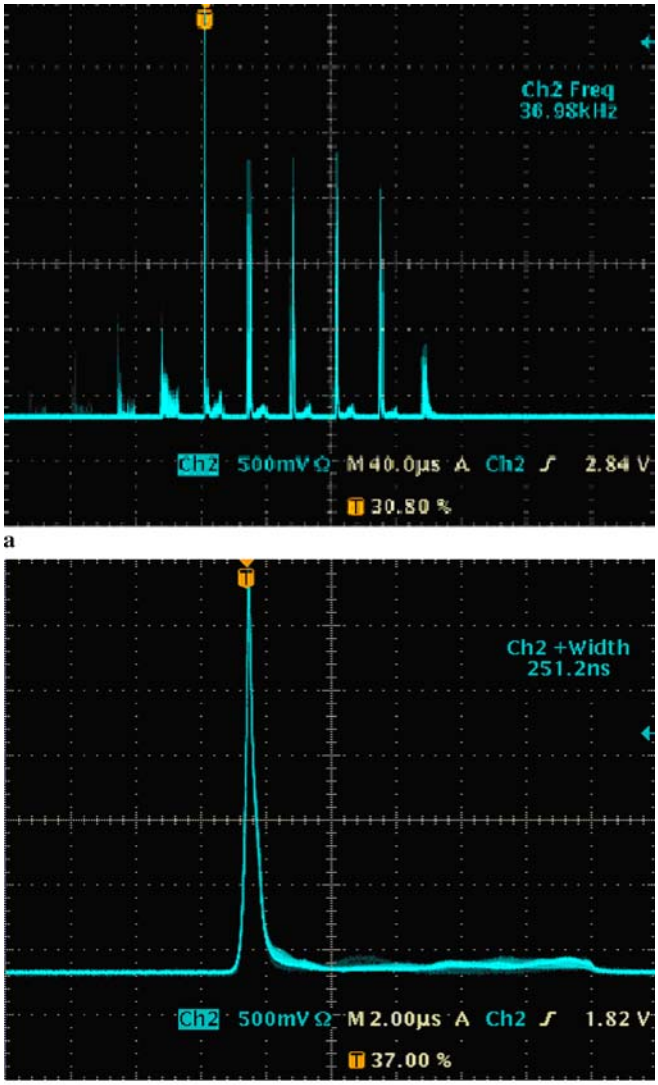

FIGURE 7 (**a**) Q-switched pulse trace for modulation frequency of 37 kHz. (**b**) A single Q-switched pulse with a pulse width of 251 nm

our pump pulse width was fixed at 200 μs, it is not possible to obtain a single Q-switched pulse for each pump pulse. There is a possibility to decrease the number of Q-switched pulses in the envelope by decreasing the pump pulse width. But, by doing so, the energy of the laser output pulses also decreases and it also becomes difficult to obtain lasing operations at wavelengths of lower gain cross sections. The number of Q-switched pulses can also be decreased by decreasing the modulation frequency of the AOQS, but it introduces instability.

The maximum peak power obtained from this scheme for the individual nanosecond pulse is about 733 W at 1318 nm, corresponding to the peak output energy of 183 μJ for an absorbed pump power of 11.5 W. Stable Q-switched operation is obtained at all the six wavelengths. The relaxation noise usually present in the free-running condition almost completely subsides in the Q-switched mode of operation. The variation of the width of the Q-switched pulse with pump diode current is shown in Fig. 8 for operation at a wavelength of 1318 nm. The observed decrease of pulse width with in-

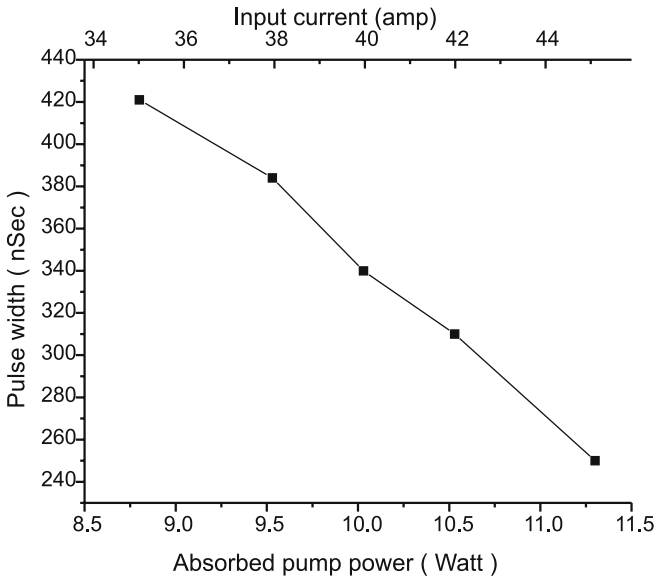

FIGURE 8 The variation of the *Q*-switched pulse width with the diode input current

crease of absorbed pump power is due to the reduced pulse build-up time.

5 Summary

An all-solid-state, side diode array pulse pumped Nd:YAG laser tunable for six wavelengths ranging from 1318.8 nm to 1356 nm was developed. The tunability is obtained by using a grating in Littrow mode. The configuration ensures a line width as low as 0.04 nm. Thermal effects limit the maximum average power to 250 mW for an average pump power of 8.0 W in the free-running condition. An acousto-optic *Q*-switching of the laser provides pulses of width 251 ns with peak power of 733 W for a average pump power of 11.5 W.

ACKNOWLEDGEMENTS DST (SP/S2/L-09/2001) and DRDO (ERIP/ER/0000149/M/01), Government of India, are acknowledged for equipment support. The authors appreciate Prof. C. Jacob, Materials Science, IIT-Kharagpur for some instrumental facilities.

REFERENCES

1 A. Rolle, Med. Laser Appl. **18**, 271 (2003)
2 A. Rolle, A. Pereszlenyi, R. Koch, M. Richard, B. Baier, J. Thorac. Cardiovasc. Surg. **31**, 1236 (2006)
3 A. Rolle, A. Pereszlenyi, R. Koch, B. Bis, B. Baier, Laser Surg. Med. **38**, 26 (2006)
4 F.X. Roux, S. Mordon, S. Mondragon, F. Sahafi, C. Fallet-Bianco, J.M. Brunetaud, Neurochirurgie **35**, 152 (1989)
5 F.X. Roux, S. Mordon, C. Fallet-Bianco, L. Merienne, B.C. Devaux, J.P. Chodkiewicz, Surg. Neurol. **34**, 402 (1990)
6 G.J. Fulchiero Jr., P.C. Parham-Vetter, S. Obagi, Dermatol. Surg. **30**, 1356 (2004)
7 D.J. Goldberg, Dermatol. Surg. **26**, 915 (2000)
8 W. Koechner, *Solid-State Laser Engineering* (Springer, Berlin Heidelberg, 1999)
9 F. Hanson, P. Poirier, J. Opt. Soc. Am. B **12**, 1311 (1995)
10 R.C. Stoneman, L. Esterowitz, Opt. Lett. **15**, 486 (1990)
11 V.V. Ter-Mikirtychnevan, V.A. Fromzel, Appl. Opt. **39**, 4964 (2000)
12 T.Y. Fan, J. Ochoa, IEEE Photon. Technol. Lett. **7**, 1137 (1995)
13 J. Marling, IEEE J. Quantum Electron. **QE-14**, 56 (1978)
14 J.E. Bernard, V.D. Lokhnygin, A.J. Alcock, Opt. Lett. **18**, 2020 (1993)
15 N.J. Vasa, M. Fujiwara, S. Yokoyama, M. Uchiumi, M. Maeda, Appl. Opt. **42**, 5512 (2003)
16 M.B. Danailov, I.Y. Milev, Appl. Phys. Lett. **61**, 746 (1992)
17 A. Saha, A. Ray, S. Mukhopadhyay, N. Sinha, P.K. Datta, P.K. Dutta, Opt. Express **14**, 4271 (2006)
18 R. Zhou, W. Wen, Z. Cai, X. Ding, P. Wang, J. Yao, Chin. Opt. Lett. **3**, 597 (2005)
19 N. Pavel, V. Lupei, T. Taira, Opt. Express **13**, 7948 (2005)
20 Z. Sun, R. Li, Y. Bi, X. Yang, Y. Bo, Y. Zhang, G. Wang, W. Zhao, H. Zhang, W. Hou, D. Cui, Z. Xu, Opt. Commun. **241**, 167 (2004)
21 C.J. Hawthorn, K.P. Weber, R.E. Scholten, Rev. Sci. Instrum. **72**, 4477 (2001)
22 D.S. Sumida, D.A. Rockwell, M.S. Mangir, IEEE J. Quantum Electron. **QE-24**, 985 (1988)
23 R. Kapoor, P.K. Mukhopadhyay, J. George, S.K. Sharma, Pramana J. Phys. **52**, 623 (1999)
24 S. Singh, R.G. Smith, L.G. van Uitert, Phys. Rev. B **10**, 2566 (1974)
25 T.W. Hansch, Appl. Opt. **11**, 895 (1972)